

Generation of wavelength-tunable, bound-state and noise-like pulses in an all-polarization-maintaining laser ring cavity based on nonlinear polarization evolution

Yazhou Shi(石亚洲), Ze Li(李泽), and Zhiguo Lv(吕志国)

Citation: Chin. Phys. B, 2026, 35 (**5**): 054202. DOI: 10.1088/1674-1056/ae15f3
http://cpb.iphy.ac.cn; http://iopscience.iop.org/cpb

What follows is a list of articles you may be interested in

Generation of ultra-flat broad spectrum with stable single-pulse mode-locking in double-clad Yb-doped fiber laser

Minghui Sun(孙铭烩), Dongxin Gao(高懂昕), Yunli Yu(于芸丽), Wenyu Wang(王文煜), Qingcao Liu(刘情操), Weixin Liu(刘维新), and Yuzhai Pan(潘玉寨)
Chin. Phys. B, 2026, 35 (**1**): 014206. DOI: 10.1088/1674-1056/adea59

Generation ofWatt-level Kerr-lens mode-locked Yb:CYA laser at 1-GHz repetition rate

Guodong Zhao(赵国栋), Junyi Ma(马骏逸), Hainian Han(韩海年), Zhaohua Wang(王兆华), and Zhiyi Wei(魏志义)
Chin. Phys. B, 2025, 34 (**8**): 084204. DOI: 10.1088/1674-1056/adcf8b

Optically pumped wavelength-tunable lasing from a GaN beam cavity with an integrated Joule heater pivoted on Si

Feifei Qin(秦飞飞), Yang Sun(孙阳), Ying Yang(杨颖), Xin Li(李欣), Xu Wang(王旭), Junfeng Lu(卢俊峰), Yongjin Wang(王永进), and Gangyi Zhu(朱刚毅)
Chin. Phys. B, 2023, 32 (**5**): 054210. DOI: 10.1088/1674-1056/acc05e

A cladding-pumping based power-scaled noise-like and dissipative soliton pulse fiber laser

Zhiguo Lv(吕志国), Hao Teng(滕浩), and Zhiyi Wei(魏志义)
Chin. Phys. B, 2023, 32 (**2**): 024207. DOI: 10.1088/1674-1056/ac8f3e

Pulse generation in Yb-doped polarization-maintaining fiber laser by nonlinear polarization evolution

Cheng-Bin Liang(梁成斌), Yan-Rong Song(宋晏蓉), Zi-Kai Dong(董自凯), Yun-Feng Wu(吴云峰), Jin-Rong Tian(田金荣), Run-Qin Xu(徐润亲)
Chin. Phys. B, 2020, 29 (**7**): 074206. DOI: 10.1088/1674-1056/ab8ac6

Generation of wavelength-tunable, bound-state and noise-like pulses in an all-polarization-maintaining laser ring cavity based on nonlinear polarization evolution

Yazhou Shi(石亚洲), Ze Li(李泽), and Zhiguo Lv(吕志国)†

School of Physical Science and Technology, Inner Mongolia University, Hohhot 010021, *China*

(Received 15 August 2025; revised manuscript received 8 October 2025; accepted manuscript online 22 October 2025)

Wavelength-tunable fiber lasers are of great interest due to their ability to meet the needs of multiple wavelengths simultaneously. In this work, a tuned spectrum of 13 nm (1564.5–1577.5 nm) is obtained using the nonlinear polarization evolution (NPE) technique by adjusting the polarization controller (PC) to use six segments of polarization-maintaining (PM) fibers with specific splicing angles in an all-PM ring cavity. The output pulse characteristics are also measured, and the signal-to-noise ratio (SNR) is greater than 74 dB. A soliton pulse with a pulse width of about 469 fs is generated at a repetition frequency of 14.12 MHz, which demonstrates the excellent performance of the fiber laser. In addition, by changing the cavity parameters and adjusting the PC, bound states and noise-like pulses are generated in the six-segment structure. So far, the generation of these two types of pulses has not been reported in other PM NPE structured fiber lasers, and the formation mechanism may be related to the complex nonlinear interactions in mode-locked fiber lasers. Our work demonstrates the potential of the PM NPE structure for applications in broad spectral tuning as well as in the generation of multiple pulse types.

Keywords: wavelength-tunable, nonlinear polarization evolution, bound states and noise-like pulses, mode-locking

PACS: 42.55.Wd, 42.60.–v, 42.60.Fc, 42.65.–k

DOI: 10.1088/1674-1056/ae15f3 **CSTR:** 32038.14.CPB.ae15f3

1. Introduction

Nowadays, ultrafast laser technology has important applications in many fields, such as ultrafast laser processing in industrial production and ultrafast laser spectroscopy in biological systems research.[1–3] The realization of passive mode-locking technique relies on saturable absorbers (SAs). Active mode-locking and passive mode-locking are the two main methods of generating pulsed lasers. Among them, passive mode-locking allows pulse widths on the order of femtoseconds and does not require any active modulation device, which is conducive to all-fiber optics. Semiconductor saturable absorber mirrors, nanomaterials, nonlinear multimode interference, nonlinear polarization evolution (NPE), nonlinear optical loop mirrors, and Mamyshev regenerators are commonly used mode-locking methods. Among these, NPE as an artificial SA has the advantages of large modulation depth and short response time. Conventional NPE mode-locking techniques use non-polarization-maintaining (non-PM) fibers, where the long-axis direction of elliptically polarized light rotates as it is transmitted through the fiber due to the Kerr effect; a polarization controller (PC) is used to filter the polarization state. However, this type of mode-locking has high temperature and stress requirements, which contributes to its poor environmental stability. In 2016, Wang *et al*. proposed a cross-splicing method to compensate for the group velocity dispersion (GVD) caused by birefringent fibers.[4] Instead of using elliptical polarization rotation in this structure, angular splicing is used to decompose the linearly polarized light into two orthogonally polarized light pulses with unequal intensities, and then the nonlinear Kerr effect (self-phase modulation and cross-phase modulation) is used to generate NPE mode-locking. However, NPE mode-locking in this structure is achieved by relying on large optical elements. In 2017, a new scheme to implement NPE in PM fibers used angular splicing between PM fibers, which greatly improved the environmental stability.[5] At the same time, the GVD introduced due to angular splicing was compensated by relying on 90° splicing between PM fiber segments of different lengths. In 2018, Szczepanek *et al*. incorporated a Faraday mirror (FM) in the PM NPE cavity, which ensured an accurate ratio of angular-spliced fiber lengths.[6]

Wavelength-tunable mode-locked fiber lasers are widely used in the fields of spectroscopy,[7] bio-imaging,[8] and material processing,[9] and effective tuning of the wavelength of passive mode-locked fiber lasers is of great research value.[10] An effective way to adjust the wavelength is to incorporate a tunable filter with a PM fiber as the main material in the laser cavity,[11] which has the advantages of low loss and high stability while ensuring the all-fiber structure. Alternatively,

†Corresponding author. E-mail: lvzhiguo@imu.edu.cn

© 2026 Chinese Physical Society and IOP Publishing Ltd. All rights, including for text and data mining, AI training, and similar technologies, are reserved.

tunable soliton pulses can be obtained by varying the temperature of the fiber in the fiber laser.[12] In 2024, the first pump power-controlled, wavelength-tunable fiber laser with a PM NPE structure was reported,[13] where a tuned spectrum of 20 nm width was obtained by varying the pump power. This demonstrates the ability of the PM NPE structure to support a wide range of tunable spectra.

In this work, a 13 nm-wide tunable spectrum is achieved by adding a PC-based all-PM laser cavity. Concurrently, the output pulse characteristics are measured, with a pulse width of approximately 469 fs and a signal-to-noise ratio (SNR) exceeding 74 dB. The high SNR indicates excellent stability of the laser cavity. Compared to other tuning methods, the use of a PC offers advantages such as low cost, low loss, compactness, and high stability. The mode-locking mechanism is based on NPE in PM fiber. When light pulses pass through PM fiber segments spliced at specific angles, NPE alters their polarization state. The modulation introduced by the PC introduces additional nonlinear phase differences, allowing the polarization state of the light pulse to be modulated again, ultimately enabling a suitable polarization state to pass through the isolator and form an artificial SA. Additionally, in the six-segment structure, by adjusting the PC, the output pulse spectral bandwidth is altered, ultimately achieving tuning. By changing the splicing angle and length of the fibers, the six-segment angle-spliced fibers are not strictly arranged in a 1:2:2:2:2:1 ratio at this point, causing the two orthogonal pulse components not to fully merge into a single beam after passing through the polarimeter and resulting in pulse separation. By carefully adjusting the PC to control the pulse polarization state, the mode-locked laser evolves into a bound-state pulse, forming noise-like pulses (NLPs) and bound-state pulses. For tightly bunched pulses, their intervals are extremely small, and their interactions primarily manifest as strong direct nonlinear effects, such as cross-phase modulation and strong coupling of gain/loss. This strongly coupled state naturally forms when the PC is tuned to maximize nonlinear polarization effects, thereby generating tightly bound pulses. For loosely bound pulses with longer intervals, direct nonlinear interactions become negligible. Adjusting the PC modifies the nonlinear phase shift and birefringence effects within the cavity, directly influencing the generation location and the intensity of dispersion waves. When the photonic crystal is tuned to a specific state, it excites dispersion waves at a defined interval, locking two pulses at a fixed large spacing to form loosely bound pulses. By adjusting the PC, the equivalent saturable absorber is set to an operating point where it is insufficient to sustain stable high-energy fundamental solitons but sufficient to initiate mode locking and maintain the macroscopic energy envelope. In this state, high pump power provides ample energy. The NPE effect, weakened by the PC, fails to effectively suppress pulse instabilities, leading to complex dynamical phenomena. Slow gain dynamics dictate the nanosecond-scale wave packet structure, manifesting energy as separated, massive pulses. Strong Kerr nonlinearity and dispersion within the wave packet dominate the formation of femtosecond-scale spike structures. Ultimately, these effects collectively drive the laser into a distinct chaotic state-a noise-like pulsed state. Our work marks the first experimental demonstration of the use of a PC for broader spectral tuning in a PM NPE structure, as well as the first generation of NLPs and bound-state pulses in such a structure, showcasing the broad application prospects of PM NPE structures in the field of wide spectral tuning.

2. Numerical simulation

The key part of the six-segment PM NPE structure is shown in Fig. 1. When the pulse passes through the first section of specially angled-spliced PM fiber, it is decomposed into two pulses whose polarizations are perpendicular to each other but whose intensities are unequal (shown by the green and red arrows in Fig. 1), and the intensities of the two pulses are related to the splicing angle. When passing through the first fiber of length L, the two pulses separate in the time domain due to GVD, and splicing with a second fiber of length $2L$ allows the two pulses to exchange their roles as fast and slow axes. The six fiber lengths are in the ratio of 1:2:2:2:2:1, which allows the lower edge of the pulse propagating in the slow axis to interact with the upper edge of the pulse propagating in the fast axis, making the nonlinear phase difference between the two pulses symmetric. Finally, after passing through the PM fiber with a specific splice angle, the two pulses are again combined into one beam. Only pulses with a specific polarization state can pass through the isolator, and the six sections of PM fiber with a specific splice angle act as an SA. If there are differences in fiber lengths, additional nonlinear phase differences are introduced, which can affect the quality of the output pulses or even generate multiple pulses. In this case, the PC compensates for the effect of fiber length by artificially stressing the fiber and introducing an additional phase delay, acting similarly to an FM; this reduces the asymmetry of the nonlinear phase between pulses due to errors in the length ratio between the PM fiber segments.

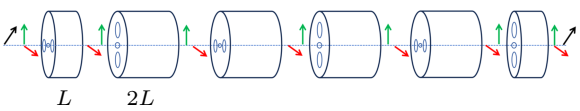


Fig. 1. Main components of six-segment PM NPE device.

The transmission spectra of the six-segment PM NPE structure are theoretically simulated to achieve dynamic tuning of the spectral bandwidth and central wavelength based on the phase difference generated by the birefringence effect. We define the output spectral bandwidth of the PM NPE structure

as the full width at half maximum of the transmission curve:

$$\Delta\lambda \cong \frac{\lambda^2}{2L\Delta n},$$

where λ is the wavelength of light, L is the length of the fiber, and n is the refractive index difference. In order to simplify the physical model and ignore the loss due to fiber fusion, each part of the transmission matrix is described by the Jones matrix, which is listed in Table 1, where θ_1 and θ_2 denote the starting and detecting angles ($\theta_1 = 30°$, $\theta_2 = 55°$), and φ_1 and φ_2 denote the phase difference in the PM fiber with length L, the PM fiber with length $2L$ ($\Delta\varphi = 2\pi nL/\lambda$). The initial condition of birefringence when there is no birefringence effect in the fiber is $n_0 = 3.6 \times 10^{-4}$, used to obtain the polarization-dependent transmission matrix

$$T = M_2F_1RF_2RF_2RF_2RF_2RF_1M_1.$$

Table 1. Jones matrix description of each part of the transmission matrix.

Jones matrices	Representation
$R = \begin{pmatrix} \cos\theta & -\sin\theta \\ \sin\theta & \cos\theta \end{pmatrix}$	Rotation matrix
$M_1 = \begin{pmatrix} \cos^2\theta_1 & \frac{1}{2}\sin 2\theta_1 \\ \frac{1}{2}\sin 2\theta_1 & \sin^2\theta_1 \end{pmatrix}$	A polarizer with a horizontal angle θ_1
$M_2 = \begin{pmatrix} \cos^2\theta_2 & \frac{1}{2}\sin 2\theta_2 \\ \frac{1}{2}\sin 2\theta_2 & \sin^2\theta_2 \end{pmatrix}$	A polarizer with a horizontal angle θ_2
$F_1 = \begin{pmatrix} e^{-\frac{i\Delta\phi_1}{2}} & 0 \\ 0 & e^{\frac{i\Delta\phi_1}{2}} \end{pmatrix}$	Fiber L horizontal in the direction of the fast axis
$F_2 = \begin{pmatrix} e^{-\frac{i\Delta\phi_2}{2}} & 0 \\ 0 & e^{\frac{i\Delta\phi_2}{2}} \end{pmatrix}$	Fiber $2L$ horizontal in the direction of the fast axis

In Fig. 2(a), the red solid line is the 2.0×10^{-4} birefringence generated by the positive-pressure PM fiber; the blue solid line is the 1.0×10^{-4} birefringence generated by the positive-pressure PM fiber; the dashed line is the 2.0005×10^{-4} birefringence generated by the positive-pressure PM fiber. The comparison of the red solid line and the blue solid line represents coarse-tuning PC, and the comparison of the dashed line and the red solid line represents fine-tuning PC. It can be seen in Fig. 2 that the spectral bandwidth and the center wavelength of the output light change significantly under the effect of coarse tuning, whereas the spectral curves produced by fine tuning change only around the original curves. In Fig. 2(b), the curve of birefringence versus spectral bandwidth of PM NPE output produced by the positive-pressure PM fiber is demonstrated, and it can be seen that the spectral bandwidth varies significantly with birefringence. The simulation results illustrate the tunability of the spectral bandwidth of the PM NPE structure, demonstrating its ability to output different laser modes with different laser spectral shapes and pulse evolution characteristics.

In the experiment, we obtained confined-state pulses within a six-segment PM NPE structure by varying the fusion angle between adjacent PM fiber segments and the length of each segment. We performed theoretical simulations of this temporal phenomenon. After passing through the angle-splitting PM fiber, the light pulse is split into two mutually perpendicular pulses, denoted as U and V, representing pulses in two orthogonal directions. The pulse propagation equations are as follows:

$$\begin{aligned}\frac{\partial U}{\partial Z} &= \frac{i\Delta\beta}{2}U - \frac{i\beta_2}{2}\frac{\partial^2 U}{\partial t^2} + \frac{g}{2}U \\ &\quad + i\gamma\left(|U|^2 + \frac{2}{3}|V|^2\right)U + \frac{i\gamma}{3}UV^2, \\ \frac{\partial V}{\partial Z} &= -\frac{i\Delta\beta}{2}U - \frac{i\beta_2}{2}\frac{\partial^2 V}{\partial t^2} + \frac{g}{2}U \\ &\quad + i\gamma\left(|V|^2 + \frac{2}{3}|U|^2\right)V + \frac{i\gamma}{3}VU^2,\end{aligned}$$

where β is the dispersion term, γ is the nonlinear term, and g represents the gain coefficient. For gain fibers, $g = 3.18$; for PM fibers, $g = 0$. The simulation results are shown in Fig. 3.

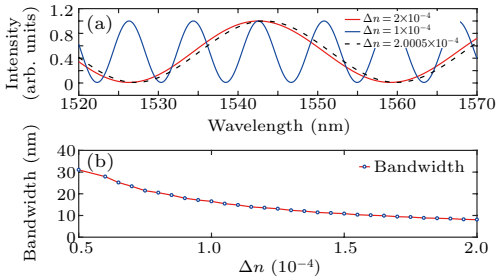


Fig. 2. (a) Calculated transmission spectra of six-segment PM NPE device. (b) Spectral bandwidth versus refractive index.

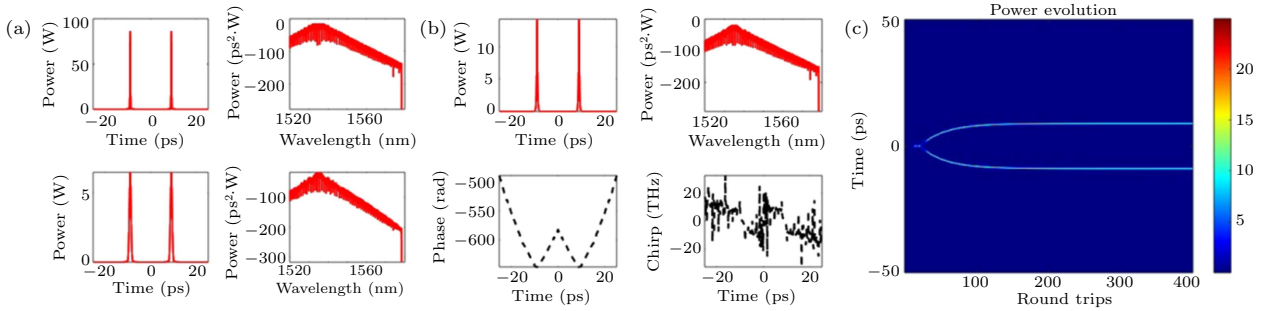


Fig. 3. (a) Time domain and spectrum in the orthogonal direction. (b) The overall time domain, spectrum, phase, and chirp. (c) The time domain pulse evolution.

3. Experimental setup

The experimental setup is shown in Fig. 4, and all the fibers and components are of PM type. The pump source is a 976 nm laser diode, and the output signal is coupled to the cavity by a wavelength division multiplexer (WDM). The gain fiber is a 1.2 m long erbium-doped fiber (EDF). An isolator (ISO) ensures unidirectional laser transmission. All the fibers and components are of PM type. The core part of the fiber laser is six sections of PM fibers (1:2:2:2:2:1), $L = 72.5$ cm, with angle splicing between two adjacent sections of PM fibers; the starting deflection angle is 30°, the checking deflection angle is 55°, and the rest of the splice angles are 90°. This constitutes an artificial SA. A PC is incorporated in the six-segment structure to regulate the polarization state of the optical signal in the fiber. A 10% output coupler (OC) is used to output the optical signal and assess the quality of the ring cavity. The total length of the fiber cavity is 15.2 m. The estimated net dispersion is -0.3258 ps^2, which is in the negative dispersion region. The output signal of the laser is detected using a spectrometer (YOKOGAWA, AQ6370D), autocorrelator (A.P.E, SM2000), radio-frequency (RF) spectrum analyzer (Keysight, N9010B), oscilloscope (RIGOL, MSO8304A), and power meter (Ophir, 50(150)A-BB-26-V1).

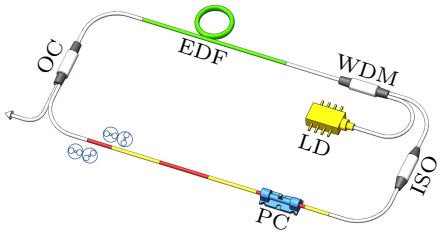


Fig. 4. Mode-locked fiber laser based on six-segment PM NPE structure.

4. Results

4.1. Generation of mode-locked and tunable spectra

Stable mode-locking is achieved by adjusting the PC at a pump power of 552 mW. Figure 5(a) demonstrates mode-locked pulse spectra with a central wavelength of 1577.5 nm and a spectral width of 12.45 nm. Figure 5(b) shows a uniform mode-locked pulse train with adjacent longitudinal mode spacing of 71.3 ns. The SNR of the radio frequency (RF) spectrum in Fig. 5(c) is about 74 dB, which indicates good laser stability. The fundamental frequency is 14.12 MHz, which corresponds well to the cavity length. In Fig. 5(d), the autocorrelation trace is fitted with sech^2 and the measured pulse width is 469 fs. In the stable mode-locked state, the PC is carefully adjusted, and it is found that the wavelength of the spectral center changes; as shown in Fig. 5(e), it gradually changes from 1577.5 nm to 1564.5 nm. The reason for this phenomenon is that the PC adjusts the polarization direction of the light pulse and uses the difference in phase delay of the PM fiber to cause light of different wavelengths to interfere constructively or destructively, thereby filtering out the target wavelength. A 13 nm wide tuned spectrum is finally obtained. In particular, each spectrum exhibits Kelly sidebands, which are characteristic of conventional solitons and correspond to resonant cavity dispersion; the Kelly sidebands are produced by interference between two closely spaced solitons. For the other spectra between 1564.5 nm and 1577.5 nm, the pulse width and repetition frequency are similar.

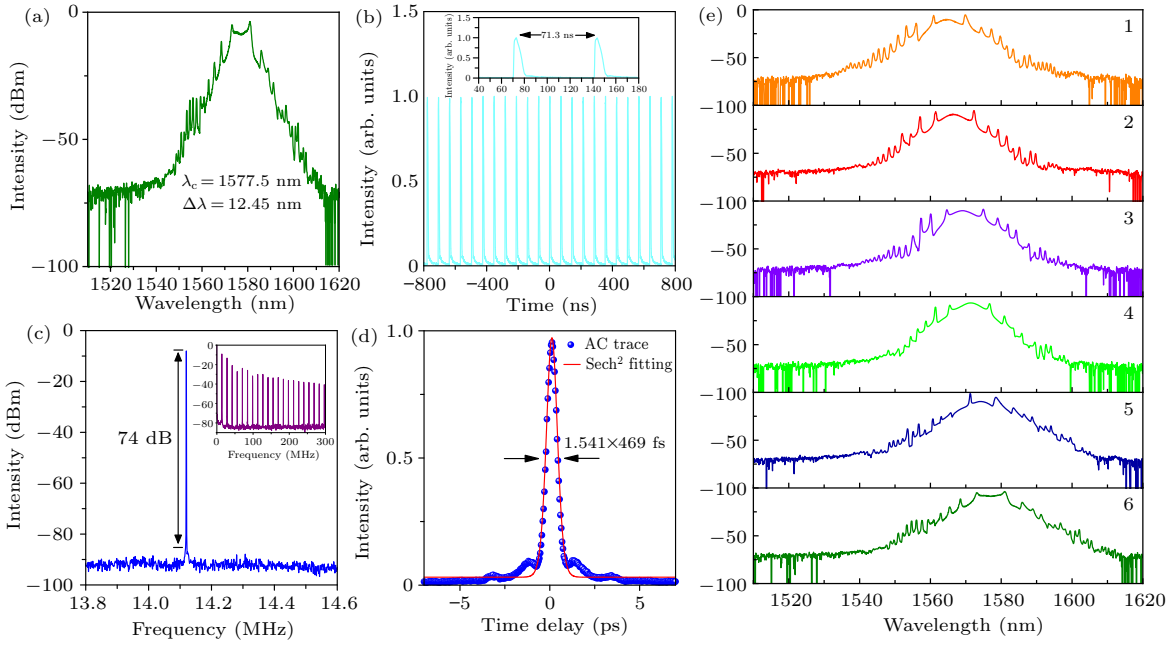


Fig. 5. (a) Mode-locked spectrum. (b) Mode-locked pulse sequences. (c) RF spectrum. (d) Autocorrelation trace and the corresponding fitting curve. (e) Tunable spectrum.

4.2. Generation of bound solitons and NLPs

Soliton pulses are typically found in the negative dispersion region and can form multiple pulses when the pump power is increased beyond a critical value due to overdriving of the mode-locking mechanism.[14] Soliton molecules or bound states are formed when multiple soliton pulses are closely spaced due to interactions.[15] Bound solitons can be categorized into tightly bound solitons and loosely bound solitons. For tightly bound soliton pairs, the time interval and the corresponding spectral modulation period are fixed. For loosely bound soliton pairs, the soliton separation is relatively loose, and the spectral modulation period is unstable. Varying the cavity parameters yields different bound solitons, including soliton pairs, soliton triplet states, and soliton quadruplet states.[16] The soliton molecule has four possible phase-locking relations, namely, $\pm\pi/2$, 0, and π. Varying the length of the individual fiber segments so that $L = 97$ cm produces a π-phase bound state at a pump power of 412 mW. We measured its output power at 6.5 mW. Modulated spectra and autocorrelation traces are shown in Fig. 6(a), which are characteristic of soliton molecules[17] and result from interference between closely spaced solitons.[18] The center wavelength of the spectrum is 1559 nm, and the spectral modulation period is 5.1 nm. Figures 6(b) and 6(c) show the pulse train and RF spectrum, respectively, with a pulse time interval of 53.6 ns. The repetition frequency is 18.45 MHz, and the fundamental frequency SNR is as high as 70 dB, which indicates stable mode-locking. Figure 6(d) shows the autocorrelation trace, where the three peaks exhibit the same pulse duration of 810 fs, with 1.28 ps separating the small and large peaks-approximately 1.58 times the pulse width-a calculation that suggests strong interactions between the soliton molecules.

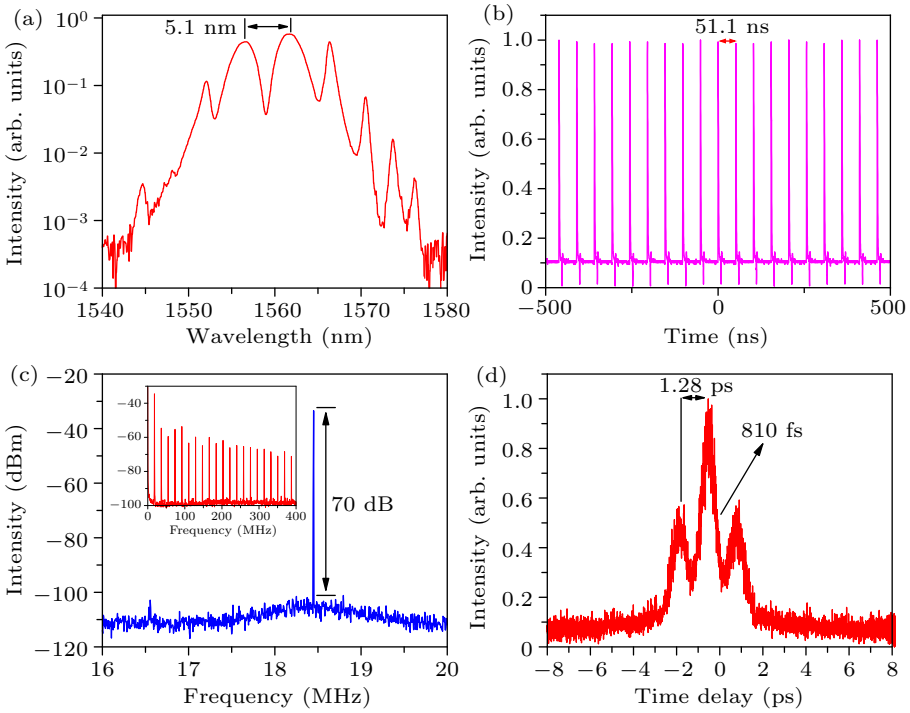


Fig. 6. (a) Tightly bound soliton spectrum. (b) Pulse sequences. (c) RF spectrum. (d) Autocorrelation trace of bound soliton.

Varying the length of the individual fiber segments so that $L = 90$ cm produces loosely bound solitons at a pump power of 179.5 mW. We measured their output power at 2.5 mW. Figure 7(a) shows the corresponding autocorrelation trace with a three-peak structure. The time interval between adjacent side peaks is 26.42 ps, and, assuming a sech^2 pulse shape, the pulse width of the center peak is 920 fs; the pulse time interval is approximately 28.72 times the pulse duration, suggesting the generation of loosely bound soliton pairs. The different peaks in the autocorrelation trace exhibit an intensity ratio of 1:2:1, which suggests the presence of secondary modulation in the detailed spectrum. The mode-locked spectra of soliton molecules centered at 1570 nm with a spectral modulation period of 0.39 nm are illustrated in Figs. 7(b) and 7(c). The emission peak of erbium-doped fiber lies near 1530–1560 nm. Any unsuppressed amplified spontaneous emission (ASE) or continuous-wave (CW) lasing in this band would exhibit significant enhancement. Through longitudinal mode competition, this ultimately forms a narrow, high-intensity CW peak directly superimposed on the pulse spectrum. We speculate that the laser may not have achieved its most stable mode-locked state. Minor perturbations, such as vibrations or temperature fluctuations, could cause the laser to switch between these two states, thereby generating CW output.

NLPs are characterized by high peak intensity, broad spectrum, and low coherence. We modulate the starting and

detection angles of the SA in the experimental setup to 23° and 45°, respectively, and change the length of the fiber segment so that $L = 58$ cm. As the fiber length decreases, the total dispersion decreases while the nonlinearity-to-dispersion ratio increases. At this point, the bound-state pulse becomes unstable. When the fiber length drops below a critical threshold, the dispersion effect weakens while nonlinear effects become dominant, completely disrupting the original bound-state equilibrium. The pulse energy fluctuates violently, and intense nonlinear effects (self-phase modulation, stimulated Raman scattering) spontaneously generate broadband noise and new frequency components. The system forms NLPs at higher energy and nonlinearity levels.

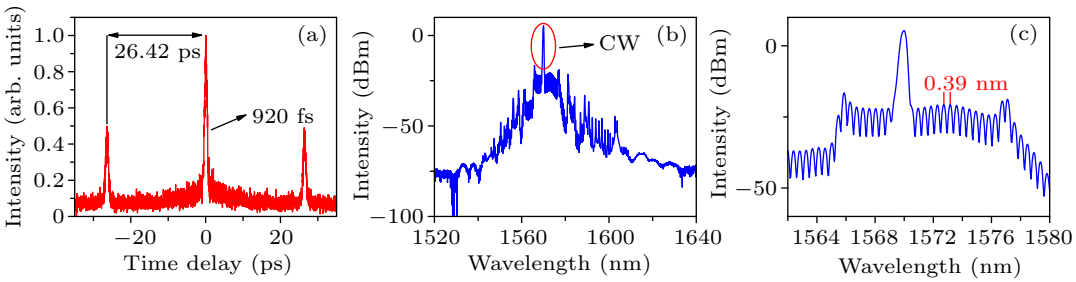


Fig. 7. Loosely bound soliton characteristics: (a) autocorrelation trace; (b) and (c) optical spectra.

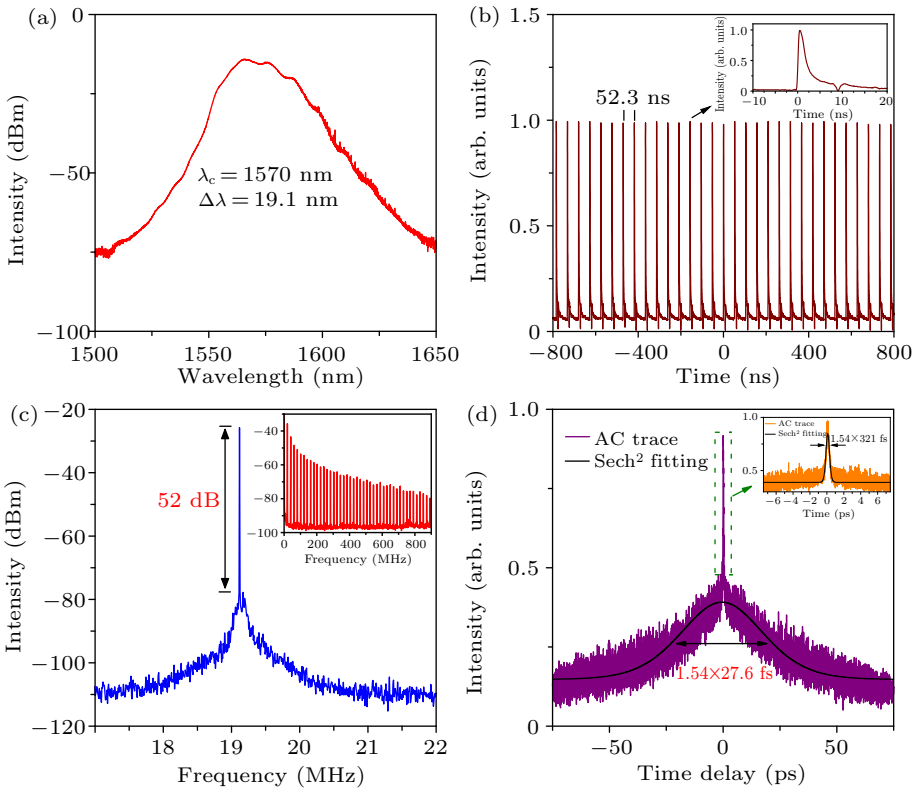


Fig. 8. (a) NLP spectrum. (b) NLP mode-locked pulse sequences. (c) RF spectrum. (d) Autocorrelation trace of large and small peaks.

Figure 8(a) shows the NLP spectrum with a center wavelength near 1570 nm and a spectral width of about 19.1 nm. The wider and smoother spectrum illustrates the low temporal coherence of the pulses, which makes them useful for many applications in optical sensing and optical metrology.[19] Figure 8(b) shows the temporal profile of the NLP, where it can be seen that the individual mode-locked pulses exhibit a long tail, formed due to long-wavelength emission in the negative dispersion cavity.[20] Figure 8(c) shows the large- and small-range RF spectra. In the inset in the upper right corner, the fundamental frequency is 19.12 MHz, and the SNR is about 52 dB. The bound-state pulse transforms into a noise-like pulse, shifting from a deterministic system with high temporal and frequency order and concentrated energy to one exhibiting high randomness. While maintaining macroscopic stability, this transformation masks microscopic disorder and diffuse energy distribution. This marks the transition of laser dynamics from an ordered state to a disordered state. The intrinsic alteration in this underlying physical mechanism directly leads to a decrease in the SNR. The autocorrelation trace of the NLP is shown in Fig. 8(d). A sharp peak as well as a broader base-typical of NLPs-can be clearly seen, and the trace is fitted

using sech2, yielding a pulse width of about 27.6 ps. Narrowing the horizontal time scale and measuring the pulse width of the spike gives 321 fs, as shown in the upper right inset.

As shown in Fig 9, to evaluate the performance of the NLP, we measured the variation of its output power with respect to the pump power. The output power increases almost linearly with the pump power without large fluctuations, confirming the stability of the NLP pulses.

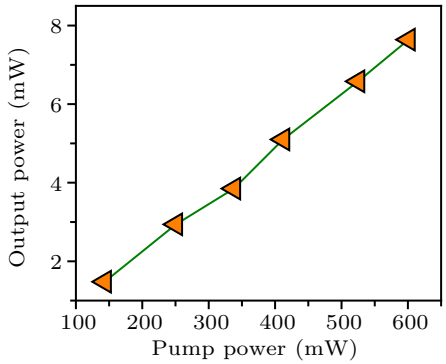


Fig. 9. Output power at different pump powers.

5. Conclusion

By adjusting the PC, a 13 nm wide tuned spectrum is obtained in a six-segment PM NPE structure using the NPE technique in all-PM fibers, and tightly bound state pulses, NLPs, and loosely bound state pulses are generated by varying the laser cavity parameters. The fiber cavity is capable of self-starting mode-locking and exhibits high stability of the output pulse. The transmission spectra of the PM NPE structure are simulated and demonstrated to enable dynamic tuning of the spectral bandwidth and center wavelength, which is experimentally confirmed. Our work shows that in the PM NPE structure, the PC can perform dynamic tuning of the laser output spectrum, promising broader tuning ranges in different bands. The NPE as a mode-locking mechanism can generate many types of pulses with a wide range of applications.

Acknowledgements

Project supported by the Natural Science Foundation of Inner Mongolia Autonomous Region of China (Grant No. 2025MS01009), the National Natural Science Foundation of China (Grant No. 12164030), and Science and Technology Plan Projects of Inner Mongolia Autonomous Region of China (Grant No. 2023KYPT0012).

References

[1] Qin M, Zhao X, Fan H, Leng R, Yu Y, Li A and Gao B 2024 *Nanomaterials* **14** 1428
[2] Sugioka K 2017 *Nanophotonics* **6** 393
[3] Uesugi Y, Miwa T, Kadoguchi N, Oya T and Yamada K 2023 *Appl. Phys. A* **129** 101
[4] Wang Y, Zhang L, Zhuo Z, Lin J, Wang Y and Zhang L 2016 *Appl. Opt.* **55** 5766
[5] Szczepanek J, Kardaś T M, Radzewicz C and Stepanenko Y 2017 *Opt. Lett.* **42** 575
[6] Szczepanek J, Kardaś T M, Radzewicz C and Stepanenko Y 2018 *Opt. Express* **26** 13590
[7] Rota-Rodrigo S, Ibañez I and López-Amo M 2013 *Appl. Phys. B* **110** 303
[8] Yamashita S and Takubo Y 2013 *Photonic Sens.* **3** 320
[9] Keller U 2003 *Nature* **424** 831
[10] Armas-Rivera I, Rodriguez-Morales L A, Durán-Sánchez M, Avazpour M, Carrascosa A, Silvestre E and Ibarra-Escamilla B 2021 *Opt. Laser Technol.* **134** 106593
[11] Luo X, Tuan T H, Saini T S, Nguyen H P T, Suzuki T and Ohishi Y 2019 *Opt. Express* **27** 14635
[12] Li J, Wang Y, Luo H, Liu Y, Yan Z, Sun Z and Zhang L 2019 *Photonics Res.* **7** 103
[13] Ye G, Liu B, Dai M, Ma Y, Shirahata T, Yamashita S and Set S Y 2024 *Opt. Lett.* **49** 2433
[14] Tang D Y, Zhao L M, Zhao B and Liu A Q 2005 *Phys. Rev. A* **72** 043816
[15] Hideur A, Ortaç B, Chartier T, Brunel M, Leblond H and Sanchez F 2003 *Opt. Commun.* **225** 71
[16] Grelu P and Soto-Crespo J M 2004 *J. Opt. B: Quantum Semiclass. Opt.* **6** S271
[17] Olivier M and Piché M 2009 *Opt. Express* **17** 405
[18] Zhu T, Wang Z, Wang D N, Yang F and Li L 2019 *Photon. Res.* **7** 61
[19] Lin A H, Chen C L, Chan C W, Chang W C and Chen Y H 2016 *Opt. Lett.* **41** 5310
[20] Meng Y, Ougrige O, Bessin F, Salhi M and Sanchez F 2024 *Appl. Phys. Lett.* **124** 201104